Strong Terahertz Radiation from a Liquid-Water Line

Liang-Liang Zhang, Wei-Min Wang, Tong Wu, Shi-Jia Feng, Kai Kang, Cun-Lin Zhang, Yan Zhang, Yu-Tong Li, Zheng-Ming Sheng, and Xi-Cheng Zhang

Phys. Rev. Applied **12**, 014005 — Published 2 July 2019

DOI: 10.1103/PhysRevApplied.12.014005

Strong Terahertz Radiation from a Liquid Water Line

Liang-Liang Zhang,[1] Wei-Min Wang,[2,3,*] Tong Wu,[4] Shi-Jia Feng,[4] Kai Kang,[1] Cun-Lin Zhang,[1] Yan Zhang,[1] Yu-Tong Li,[3,5] Zheng-Ming Sheng,[6,7,5,8,†] and Xi-Cheng Zhang[9,1]

[1]*Beijing Advanced Innovation Center for Imaging Theory and Technology and Key Laboratory of Terahertz Optoelectronics (MoE), Department of Physics, Capital Normal University, Beijing 100048, China*

[2]*Department of Physics, Renmin University of China, Beijing 100872, China*

[3]*Beijing National Laboratory for Condensed Matter Physics, Institute of Physics, CAS, Beijing 100190, China*

[4]*Beijing Key Laboratory for Precision Optoelectronic Measurement Instrument and Technology, School of Optoelectronics, Beijing Institute of Technology, Beijing 100081, China*

[5]*IFSA Collaborative Innovation Center, Shanghai Jiao Tong University, Shanghai 200240, China*

[6]*SUPA, Department of Physics, University of Strathclyde, Glasgow G4 0NG, United Kingdom*

[7]*Key Laboratory for Laser Plasmas (MoE) and School of Physics and Astronomy, Shanghai Jiao Tong University, Shanghai 200240, China*

[8]*Tsung-Dao Lee Institute, Shanghai 200240, China*

[9]*The Institute of Optics, University of Rochester, Rochester, New York 14627, USA*

Abstract

Terahertz radiation generation from liquid water has long been considered impossible due to strong absorption. A few very recent works reported terahertz generation from water, but the mechanism is not clear and the efficiency demands to be enhanced. We show experimentally that strong single-cycle terahertz radiation with field strength of 0.2 MVcm^{-1} is generated from a water line/column of $\sim 200\mu m$ in diameter irradiated by a mJ femtosecond laser beam. This strength is 100-fold higher than that produced from air using single color pumping. We attribute the mechanism to the laser-ponderomotive-force-induced current with the symmetry broken around the water-column interface. This mechanism can explain our following observations: the radiation can be generated only when the laser propagation axis deviates from the column center; the deviation determines its field strength and polarity; it is always p-polarized no matter whether the laser is p- or s-polarized. This study provides a simple and efficient scheme of table-top terahertz sources based on liquid water.

PACS numbers: 42.65.Re, 32.80.Fb, 52.38.-r, 52.65.Rr

* weiminwang1@ruc.edu.cn

† z.sheng@strath.ac.uk

I. INTRODUCTION

Achieving table-top terahertz (THz) sources with high field strength and broad bandwidth is an outstanding issue in THz science. Such sources can find applications in material research [1, 2], biomedical imaging [3], non-destructive detection [4], and THz-field interaction with matter [5, 6]. Previous studies have demonstrated THz generation from solids [8–11] and gases [12–22] via different mechanisms. However, THz generation from liquid, in particular water, has long been considered impossible because of its strong absorption of THz radiation. Therefore, how to generate THz radiation from water is a great challenge for both basic and applied research. In 2017, two groups reported THz emission from liquid water [23, 24]. When an intense laser beam of tens of mJ was focused on liquid water in a cuvette, extreme broadband THz radiation was generated [23], where it is considered that laser spectral broadening played a key role. In the other work [24], when a mJ laser beam irradiated a water film with the thickness ~ 200 μm, THz radiation was produced with 1.8 times higher strength than that produced from air. So far, the THz radiation mechanism in water has not yet been well clarified and the yield efficiency demands to be further enhanced.

Here, we demonstrate experimentally that the efficiency can be enhanced by three orders of magnitude when a water column with the diameter ~ 200 μm is adopted. With a mJ femotsecond laser beam, the THz field strength can reach 0.2 MVcm^{-1} which is as high as generated via the standard two-color laser scheme in air [12, 13]. To explain our result, we propose that the THz radiation originates from a net current formed due to the presence of the column interface. The laser self-focusing in water causes a plasma to be produced. The laser ponderomotive force forms positive and negative currents distributed on two sides of the laser propagation axis, respectively. The symmetry of the two currents can be broken provided the laser axis deviates from the water column center. As the deviation grows, the net current and resulting THz radiation will be enhanced. This mechanism implies that the THz polarization is on the column cross-section plane and its strength scales linearly with the laser energy. These are verified by our experiments and particle-in-cell (PIC) simulations.

II. EXPERIMENTAL SETUP

Figure 1 shows the experimental schematic, where a laser beam is incident along the $+z$ direction and the water column axis is along the y direction. The laser beam is delivered from a Ti:Sapphire amplifier (Spitfire, Spectra Physics) with a central wavelength 800nm, pulse duration 100fs, and repetition rate 1kHz. It is split into pump and probe beams with controllable time delay. The pump beam is focused by an off-axis parabolic mirror (PM1) with 1-inch equivalent focal length. The polarization of the pump beam is linear and its orientation can be rotated through a half-wave plate. A liquid geyser with a pressure of 0.1MPa creates a free-flowing water column with the diameter ~ 200 μm near the tip of the geyser. The water column is located around the focusing plane of the pump beam and can precisely move along the x direction (equivalent to the shift of the laser propagation axis). Here, we fix the coordinate on the column and set the column center as the origin, as shown in the inset.

The THz pulse is collimated and refocused by two parabolic mirrors. Filters and two wire-grid THz polarizers are placed in the THz path to block the residual laser beam and avoid over rotation of the detection crystal. The probe beam passes through a pair of climbing mirrors and then is focused by a 125mm convex lens. It co-propagates with the THz pulse by passing through a hole drilled on the back of the parabolic mirror (PM3). The collection portion is installed on a platform which can be rotated around the water column to detect the THz pulse at an angle θ (positive: anti-clockwise) with respect to the laser incident direction. To compensate the polarization rotation of the probe beam when the platform rotates, a polarizer and a half-waveplate are placed in the probe beam path. The THz fields resolved traces are obtained through electro-optic (EO) sampling with a 3 mm thick $\langle 110 \rangle$-cut ZnTe crystal as the detector [25] to compare the THz radiations emitted from air, water film and water column under the same detection scheme. It is necessary to use thicker crystal to reach high dynamic range of the THz waveform. We had tried to use 300um-thick GaP as the detector, but no THz signal was detectable from the air case. To avoid the over rotation and to reduce the THz intensity inside the 3mm-thick ZnTe crystal, we placed two wire-grid polarizers in the THz path. By retrieving the THz waveform by the EO sampling, we can estimate the electric field according to the rotation angle of the THz polarizer. In our experiments, the laser beam is taken as 2 mJ energy, p-polarization (along

the x direction), the laser propagation axis is displaced 60 μm ($x_L = 60$ μm) from the water column center, and the THz pulse is collected at $\theta = 0°$, except in Fig. 6.

III. DEMONSTRATION OF THZ GENERATION

Figure 2(a) shows the waveform of the THz pulse generated from the water column. As comparison, the ones from water film and air irradiated by the same laser beam are also displayed in Figs. 2(b) and 2(c). The THz pulse from the water column has a field strength 0.15 MVcm^{-1}, 20-fold and 100-fold higher than the one from the water film and air, respectively. The THz strength is as high as the one with the standard two-color laser scheme in air [12, 13] even though a one-color laser beam is used here. Note that the strength can be enhanced to 0.2 MVcm^{-1} when the THz pulse is collected at θ of $40° - 60°$ rather than $\theta = 0°$ [see Fig. 6]. In Fig. 2(b) we take a 200-μm-thick and 5-mm-wide water film, which is produced by a jet nozzle with polished sapphire surfaces. The laser incident angle is taken as 60° to optimize the THz strength, in particular, nearly no THz generation with the laser normal incidence [24]. However, in the water column case, the normal laser incidence along the $+z$ direction is always taken in our experiments and efficient THz generation is observed (we expect the laser beam travels along the z-axis due to its intensity $\sim 10^{15}$ Wcm^{-2} and the water-plasma with a length ~ 100 μm). This suggests there are different generation mechanisms in the two cases [different THz strength scaling is also observed in Fig. 4].

The THz spectra are shown in Fig. 2(d). One can observe that the spectrum for the water column is the narrowest and the one for air is widest. Assuming that the THz radiation from the water film and air can be also attributed to net currents formed in plasma (the mechanism in the film case is not clear), one could explain the differences appearing in the spectra by differences in plasma density profiles and lengths formed in the three cases. The spectra could suggest that in air, the formed plasma could be the longest and have the most complex density profile (or the worst density uniformity); In the water column, the formed plasma could be the shortest and have the best density uniformity. According to the definition of the dynamic range in Ref. [26], the calculated dynamic ranges of the three waveforms are 50 (air), 63 (water film) and 160 (water line), respectively. Note that these dynamic ranges are not large because the THz signals are attenuated by two wire-grid polarizers to avoid over rotation of the detection crystal.

IV. MECHANISM

The mechanism can be explained as the laser-ponderomotive-force-induced current with the symmetry broken around the column interface. Figure 3(a) shows that the two THz waveforms are roughly anti-symmetric when the laser axis deviates from the column center by $+60\mu m$ and $-60\mu m$ ($x_L = \pm 60\mu m$), respectively. While the laser axis is at the column center ($x_L = 0$), virtually no THz pulse is generated, as seen in Fig. 3(b). As $|x_L|$ is increased, the amplitude is first enhanced and then lowered. The amplitude peaks appear around $x_L = \pm(60\mu m \sim 70\mu m)$. These are in agreement with our PIC simulation results shown by the line in Fig. 3(b).

Our simulations are performed with the KLAPS code [27], in which we adopt the same parameters of the water column and laser (energy, duration, and polarization) as in the experiments. The code has been applied in THz generation from laser-driven gas and plasma [18, 22, 28], which includes field ionization realized by Monte Carlo method, movement of the created electrons and ions computed by the relativistic motion equation, and a full-Maxwell-equation solver to calculate electromagnetic fields. Considering that the laser self-focusing in water should be stronger than in air, we assume that the laser beam in the water column has the spot radius $w_0 = 30$ μm. Then, the corresponding intensity is 1.5×10^{14} Wcm^{-2} $- 1.7 \times 10^{15}$ Wcm^{-2} when the laser energy varies within 0.2 mJ $-$ 2.4 mJ. In our simulations, the laser energy is taken as 2mJ (1.2×10^{15} Wcm^{-2}) except Fig. 4. With such laser intensities, plasma is quickly produced via laser-field ionization. No net current can be formed via the ionization since the symmetry of the ionization by a one-color 800nm laser beam is not broken [17, 28].

Our simulations shown in Fig. 3(c) suggest that net currents can be formed in the laser interactions with the water-column plasma. We examine the quasi-static currents $\langle J_x \rangle$, $\langle J_y \rangle$, and $\langle J_z \rangle$, respectively, where these currents are obtained by temporally averaging J_x, J_y, and J_z over one laser cycle. Here, the laser polarization is along the x direction (p-polarization). One can see in Fig. 3(c) that the total/net currents $\sum \langle J_x \rangle \neq 0$ unless $x_L = 0$, where $\sum$ means spatial summation. When $x_L = 0$, the positive and negative currents are symmetrically distributed, therefore, the net current is zero. When $x_L = 20$ μm, the positive current is distributed within a larger area than the negative one, therefore, the net current is positive. While $x_L = -20$ μm, the positive current is distributed within a smaller area,

therefore, the net current is negative. In addition, the net currents $\sum\langle J_y\rangle$ and $\sum\langle J_z\rangle$ remain zero with any x_L, as in usual cases without special target interfaces.

Besides the column interface in the laser incident plane, $\sum\langle J_x\rangle \neq 0$ is also due to the transverse non-uniformity of laser intensity. With a Gaussian laser beam, the laser ponderomotive force [29] pushes the plasma electrons away from the laser axis. Hence, the quasi-static current is negative on the upper($x > x_L$) and positive on the lower ($x < x_L$). Around the column interface, the pushed electrons are pulled back by the plasma ions due to strong charge-separation fields. This prevents the electrons from escaping away from the interface, constraining the current near the interface. Hence, the interface breaks the symmetry between the positive and negative currents. The area difference between the positive and negative currents can be estimated with

$$\Delta S = 2f(x_L) - f(x_L + w) - f(x_L - w), \tag{1}$$

where $f(x) = [x\sqrt{R^2 - x^2} + R^2 \arcsin(x/R)]/2$, R is the column radius and w is the efficient width of the laser beam (w at the order of w_0). Obviously, $|\Delta S|$ grows with increasing $|x_L|$. Provided x_L is replaced by $-x_L$, the absolute value of ΔS remains constant, but its sign is reversed. This can explain the experimental and PIC results within $|x_L| < x_L^{opt}$ shown in Fig. 3(b) (THz peaks at $\pm x_L^{opt}$), since $J_{net} \propto \Delta S$ and $E_{THz} \propto J_{net}$ [18, 22]. Note that experimental results deviated from the theoretical ones could be ascribed to tolerances in the laser lateral shift and fluctuations of the water column surface. Similar to the two-color scheme in air [17, 19], THz pulses can be generated once net currents are formed in plasma due to the plasma modulation [18], which causes single-cycle THz waveforms [see Figs. 2(a),3(a)]. The estimation of ΔS in the laser-entrance side can be applied in the laser-exit side since the laser beam is normally incident.

Figure 3(b) also shows that there are optimized values of x_L for the THz field strength. This is because the laser-water interaction zone becomes too small if $|x_L|$ is taken as a large value, which limits the THz generation. According to our PIC simulations, x_L^{opt} depends on the laser spot radius w_0: $x_L^{opt} \simeq 92\mu m$ with $w_0 = 15\mu m$, $x_L^{opt} \simeq 80\mu m$ with $w_0 = 30\mu m$ [see Fig. 3(b)], and $x_L^{opt} \simeq 70\mu m$ with $w_0 = 45\mu m$. Based on the simulation results, we could roughly summarize as $x_L^{opt} \simeq R - 2w_0/3$. This value varies slightly with the laser energy within the range of 0.2mJ to 2.4mJ.

V. THZ STRENGTH SCALING AND POLARIZATION

The THz field strength scaling with the laser intensity or energy is determined by the ponderomotive force. In a laser field, motion of an electron is governed by the Hamiltonian $H = mc^2\gamma - e\varphi$, where $\mathbf{p}$ and $\gamma = \sqrt{1 + (\mathbf{p}/mc)^2}$ are the momentum and relativistic factor, respectively, e and m are the electron charge and mass, respectively, c is the light speed in vacuum, and φ is the scalar potential generated due to the plasma response. Taking the spatial derivative of H, one can obtain $dp_z/dt = \partial(e\varphi - mc^2\gamma)/\partial z$ and $d(\mathbf{p}_\perp - e\mathbf{A}/c)/dt = \nabla_\perp(e\varphi - mc^2\gamma)$, where $\mathbf{A}$ is the laser vector potential. We consider a plasma with the plasma oscillating frequency $\omega_p = \sqrt{4\pi e^2 n_e/m}$ much lower than the laser frequency ω, where n_e is the plasma density. Due to $\omega_p \ll \omega$ here, one can assume that any physical quantity Q in this laser-plasma system can be divided into a fast varying part and a slowly varying part, i.e., $Q = Q^f + \langle Q\rangle$, where Q^f varies at the order of ω, $\langle Q\rangle$ at the order of ω_p, $\langle Q\rangle = \int_0^T Q dt/T$, and $T = 2\pi/\omega$ is the laser cycle. The fast varying part of the momentum satisfies $dp_z^f/dt = -mc^2\partial\gamma^f/\partial z$ and $d(\mathbf{p}_\perp^f - e\mathbf{A}/c)/dt = 0$. The slowly varying part satisfies $d\langle\mathbf{p}_\perp\rangle/dt = e\nabla_\perp\varphi - mc^2\nabla_\perp\langle\gamma\rangle$, where the first term on the right hand is the electrostatic force and the second is the ponderomotive force $\mathbf{F}_p$. In our case with $\omega_p \ll \omega$, basically $|\langle\mathbf{p}\rangle| \ll |\mathbf{p}^f|$ and $|e\nabla_\perp\varphi| \ll F_p$. Therefore, $\gamma \simeq 1 + e^2\mathbf{A}^2/2m^2c^4$ [30] and $d\langle\mathbf{p}_\perp\rangle/dt \simeq \mathbf{F}_p = -e^2\nabla_\perp\langle\mathbf{A}^2\rangle/2mc^2$. By applying $\langle\mathbf{J}_\perp\rangle = -en_e\langle\mathbf{p}_\perp\rangle/m$ in a non-relativistic case, the quasi-static current induced by the ponderomotive force is given by

$$\langle\frac{\partial\mathbf{J}_\perp}{\partial t}\rangle \simeq \frac{e^3 n_e}{2m^2c^2}\nabla_\perp\langle\mathbf{A}^2\rangle. \tag{2}$$

This equation gives $\langle\partial\mathbf{J}_\perp/\partial t\rangle \propto A_0^2/w_0^2 \propto \varepsilon_{laser}/w_0^2$, where we consider a Gaussian beam with $\nabla_\perp\langle\mathbf{A}^2\rangle \sim A_0^2/w_0^2$ and the lase energy $\varepsilon_{laser} \propto A_0^2$. According to $\mathbf{E}_{THz} \propto \langle\partial\mathbf{J}_\perp/\partial t\rangle$ [18, 22], one can obtain:

$$E_{THz} \propto \frac{\varepsilon_{laser} n_e}{w_0^2}. \tag{3}$$

This linear scaling of the THz field strength with the laser energy roughly agrees with our experimental and PIC results as shown in Fig. 4. Note that this scaling is different from that in the water film case [24], in which $E_{THz} \propto \sqrt{\varepsilon_{laser}}$. Below 1.4 mJ laser energies, the THz amplitude follows a linear scaling with a slower increasing rate than those for higher laser energies. According to Eq. (3) one could explain the two-region linear scaling as w_0 decreases and n_e increases with higher laser energy. Note that n_e is slightly changed when the

laser energy is taken between 0.2mJ and 2.4mJ with the intensity around 2×10^{14} W/cm $-$ 1.7×10^{15} Wcm^{-2}. In this intensity range, the first order of complete ionization occurs for oxygen and hydrogen, but the second order of ionization of oxygen is not strong because it requires an intensity above 2×10^{15} Wcm^{-2}. Our PIC simulation results roughly follow the scaling with $1/w_0^2$. For example, the net currents with $w_0 = 15\mu m$ is 3-6 times (varying with x_L) of those with $w_0 = 30\mu m$ when the laser intensity is fixed. The deviation from the predicted value 4 could be explained as ΔS also depends on w_0 and x_L.

The ponderomotive-induced current given in equation (2) is symmetric in any transverse direction, e.g., it is negative at $y > 0$ and positive at $y < 0$, which exactly counteract each other. Hence, no net current can be formed in a transverse direction, except in the x direction. In this direction, the symmetry of the current can be broken by the water-column interface, as shown in Fig. 3(c). As a result, the THz polarization is always along the x direction (p-polarized), no matter whether the laser beam is taken as p-polarization or not. This is verified by our experiments, as shown in Fig. 5. We record the transverse components of the THz electric field by electro-optic sampling and then obtain the polarization trajectory by recomposing the THz fields. When we change the laser polarization angle from 0° (p-polarized) to 90° (s-polarized), the THz pulse keeps p-polarized. These experimental results are reproduced by our PIC simulations.

Figure 6 shows the angular distribution of the THz pulses in the range of $0° - 90°$. The THz pulses are stronger with $x_L = -60\mu$m than those with $x_L = 60\mu$m. This is because the detector is located at $x < 0$ (see Fig. 1). The THz pulses with $x_L = 60\mu$m propagate a longer distance to the detector, which causes stronger absorption. With $x_L = -60\mu$m the peak angles appear around $40° - 60°$. In this case, the pulses propagate mainly in the plasma towards the detector. Considering that the net current is along the x direction, the strongest emission from the current should be at $\theta = 0°$ and it weakens with increasing θ. On the other hand, with $\theta = 0°$ the THz pulse propagates the longest distance in the plasma and it is most strongly absorbed and scattered by the plasma. The propagation distance and the absorption decreases with increasing θ. The two factors cause the strongest THz pulses to be observed at $40° - 60°$. These factors can also explain the energy decline from $\theta = 0°$ to 30° in the case with $x_L = 60\mu$m. However, paths of the pulses detected at larger θ are difficult to obtained because they are affected by scattering and refraction at plasma-water and water-air boundaries and they significantly deviate from the initial emission direction.

Finally, according to Fig. 6 we calculate the THz yield efficiency to be above 6×10^{-5}, which is as high as that with the two-color scheme pumped by 800nm lasers [20, 31].

VI. WATER COLUMN CHARACTERISTICS IN OUR EXPERIMENTS

We evaluate the diameter of the water column according to the diameter of the liquid geyser aperture. The laser beam is focused at the spot near the tip of the liquid geyser (about 5 mm to the geyser tip). As shown in Fig. 7 taken in our measurements, the water column has smooth surface and keeps a uniform shape. With the gravity of the flowing liquid considered, the water column diameters at the geyser tip and laser focus have a difference less than 1% (or $2\mu m$). Therefore, one can evaluate the water column diameter by the aperture of the liquid geyser. It is not easy to tailore the column diameter due to the complex fabrication of a high quality liquid geyser. The shape and smoothness of the geyser tip decide the formation of the water column.

The flow rate of the flowing jet in our experiments is taken as 0.015 L/min (corresponding to 2m/s). There is an optimum value within the range of 0.01-0.02 L/min. Within this range, both the obtained water column and the THz signal are stable. With a value higher than 0.02 L/min, the water column will be out of shape and even appear atomization. With a value lower than 0.01 L/min, the water column will become discontinuous.

The plasma is formed by a laser beam of 100 fs via field ionization. During the laser interactions with the water column and plasma, the plasma should remain the column profile since the plasma expansion speed is low. In our case with the laser intensity around 10^{15} $\mathrm{Wcm^{-2}}$ the ion sound velocity is low, which determines the plasma expansion speed.

VII. CONCLUSION

In summary, we have proposed an efficient scheme to generate liquid-water-based THz radiation with a single laser beam, where the field strength and yield efficiency are as high as the standard two-color laser scheme in gases. Our experiments have shown that a water column irradiated by a 800 nm one-color laser beam of 2 mJ can emit broadband THz radiation with a strength 0.2 $\mathrm{MVcm^{-1}}$, two orders of magnitude higher than one from air or a water film. A laser-ponderomotive-force-induced current model has been proposed to

explain the THz generation mechanism. The model predicts the dependence of the THz generation on laser energy, polarization, as well as the deviation between the laser axis and the column center, which has been verified by our experiments and PIC simulations. In particular, the THz field strength and even polarity can be controlled by the deviation.

ACKNOWLEDGMENTS

This work was supported by Beijing Natural Science Foundation (Grant No. JQ18015), National Key R&D Program of China (Grant No. 2018YFA0404801), National Natural Science Foundation of China (Grants No. 11775302 and 11721091), and Science Challenge Project of China (Grant No. TZ2016005 and TZ2018005). X.-C. Z. was also partially sponsored by the Army Research Office and was accomplished under Grant No. US ARMY W911NF-17-1-0428. We thank Prof. David R. Jones for useful discussion.

---

[1] B. Ferguson and X.-C Zhang, Materials for terahertz science and technology, Nat. Mater. **1**, 26 (2002).

[2] B. Clough, J. Dai, and X.-C. Zhang, Laser air photonics: beyond the terahertz gap, Mater. Today **15**, 50 (2012).

[3] D. Mittleman, *Sensing with Terahertz Radiation* (Springer-Verlag, 2003).

[4] M. Tonouchi, Cutting-edge terahertz technology, Nat. Photonics **1**, 97 (2007).

[5] T. Kampfrath, K. Tanaka, and K. Nelson, Resonant and nonresonant control over matter and light by intense terahertz transients, Nat. Photonics **7**, 680 (2013).

[6] S. Spielman, B. Parks, J. Orenstein, D. T. Nemeth, F. Ludwig, J. Clarke, P. Merchant, and D. J. Lew, Observation of the Quasiparticle Hall Effect in Superconducting $YBa_2Cu_3O_{7-\delta}$, Phys. Rev. Lett. **73**, 1537 (1994).

[7] F. Blanchard, G. Sharma, L. Razzari, X. Ropagnol, H.-C. Bandulet, F. Vidal, R. Morandotti, J.-C. Kieffer, T. Ozaki, and H. Tiedje, Generation of intense terahertz radiation via optical methods, IEEE J. Sel. Top. Quantum Electron. **17**, 5 (2011).

[8] Z. Jin, Z. L. Chen, H. B. Zhuo, A. Kon, M. Nakatsutsumi, H. B. Wang, B. H. Zhang, Y. Q. Gu, Y. C. Wu, B. Zhu, L. Wang, M. Y. Yu, Z. M. Sheng, and R. Kodama, Tunable radiation

source by coupling laser-plasma-generated electrons to a periodic structure, Phys. Rev. Lett. **107**, 265003 (2011).

[9] J. A. Fulop, L. Palfalvi, M. C. Hoffmann, and J. Hebling, Towards generation of mJ-level ultrashort THz pulses by optical rectification, Opt. Express **19**, 15090 (2011).

[10] A. Gopal, S. Herzer, A. Schmidt, P. Singh, A. Reinhard, W. Ziegler, D. Brommel, A. Karmakar, P. Gibbon, U. Dillner et al., Observation of gigawatt-class THz pulses from a compact laser-driven particle accelerator, Phys. Rev. Lett. **111**, 074802 (2013).

[11] G.-Q. Liao, Y.-T. Li, Y.-H. Zhang, H. Liu, X.-L. Ge, S. Yang, W.-Q. Wei, X.-H. Yuan, Y.-Q. Deng, B.-J. Zhu, Z. Zhang, W.-M. Wang, Z.-M. Sheng, L.-M. Chen, X. Lu, J.-L. Ma, X. Wang, and J. Zhang, Demonstration of coherent terahertz transition radiation from relativistic laser-solid interactions, Phys. Rev. Lett. **116**, 205003 (2016).

[12] D. J. Cook and R. M. Hochstrasser, Intense terahertz pulses by four-wave rectification in air, Opt. Lett. **25**, 1210 (2000).

[13] M. Kress, T. Loffler, S. Eden, M. Thomson, and H. G. Roskos, Terahertz-pulse generation by photoionization of air with laser pulses composed of both fundamental and second-harmonic waves, Opt. Lett. **29**, 1120 (2004).

[14] X. Xie, J. Dai, and X.-C. Zhang, Coherent control of THz wave generation in ambient air, Phys. Rev. Lett. **96**, 075005 (2006).

[15] K. Y. Kim, A. J. Taylor, J. H. Glownia, and G. Rodriguez, Coherent control of terahertz supercontinuum generation in ultrafast laser-gas interactions, Nat. Photonics **2**, 605 (2008).

[16] H. C. Wu, J. Meyer-ter-Vehn, and Z. M. Sheng, Phase-sensitive terahertz emission from gas targets irradiated by few-cycle laser pulses, New J. Phys. **10**, 043001 (2008).

[17] K. Y. Kim, J. H. Glownia, A. J. Taylor and G. Rodriguez, Terahertz emission from ultrafast ionizing air in symmetry-broken laser fields, Opt. Express **15**, 4577 (2007).

[18] W.-M. Wang, Z.-M. Sheng, H.-C. Wu, M. Chen, C. Li, J. Zhang, and K. Mima, Strong terahertz pulse generation by chirped laser pulses in tenuous gases, Opt. Express **16**, 16999 (2008).

[19] I. Babushkin, W. Kuehn, C. Kohler, S. Skupin, L. Berge, K. Reimann, M. Woerner, J. Herrmann, and T. Elsaesser, Ultrafast spatiotemporal dynamics of terahertz generation by ionizing two-color femtosecond pulses in gases, Phys. Rev. Lett. **105**, 053903 (2010).

[20] M. Clerici, M. Peccianti, B. E. Schmidt, L. Caspani, M. Shalaby, M. Giguere, A. Lotti, A. Couairon, F. Legare, T. Ozaki, D. Faccio, and R. Morandotti, Wavelength scaling of terahertz generation by gas ionization, Phys. Rev. Lett. **110**, 253901 (2013).

[21] V. A. Andreeva, O. G. Kosareva, N. A. Panov, D. E. Shipilo, P. M. Solyankin, M. N. Esaulkov, P. Gonzalez de Alaiza Martinez, A. P. Shkurinov, V. A. Makarov, L. Berge, and S. L. Chin, Ultrabroad terahertz spectrum generation from an air-based filament plasma, Phys. Rev. Lett. **116**, 063902 (2016).

[22] L.-L. Zhang, W.-M. Wang, T. Wu, R. Zhang, S.-J. Zhang, C.-L. Zhang, Y. Zhang, Z.-M. Sheng, and X.-C. Zhang, Observation of terahertz radiation via the two-color laser scheme with uncommon frequency ratios, Phys. Rev. Lett. **119**, 235001 (2017).

[23] I. Dey, K. Jana, V. Yu. Fedorov, A. D. Koulouklidis, A. Mondal, M. Shaikh, D. Sarkar, A. D. Lad, S. Tzortzakis, A. Couairon, G. R. Kumar, Highly efficient broadband terahertz generation from ultrashort laser filamentation in liquids, Nat. Commun. **8**, 1184 (2017).

[24] Q. Jin , Y. E, K. Williams, J. Dai, and X.-C. Zhang, Observation of broadband terahertz wave generation from liquid water, Appl. Phys. Lett. **111**, 071103 (2017).

[25] Q. Wu and X.-C. Zhang, Free-space electro-optic sampling of terahertz beams, Appl. Phys. Lett. **67**, 3523 (1995).

[26] M. Naftaly and R. Dudley, Methodologies for determining the dynamic ranges and signal-to-noise ratios of terahertz time-domain spectrometers, Opt. Lett. **34**, 1213 (2009).

[27] W.-M. Wang, P. Gibbon, Z.-M. Sheng, and Y.-T. Li, Integrated simulation approach for laser-driven fast ignition, Phys. Rev. E **91**, 013101 (2015).

[28] W.-M. Wang, S. Kawata, Z.-M. Sheng, Y.-T. Li, J. Zhang, L. M. Chen, L. J. Qian, J. Zhang, Efficient terahertz emission by mid-infrared laser pulses from gas targets, Opt. Lett. **36**, 2608 (2011).

[29] P. Gibbon, *Short Pulse Laser Interactions with Matter* (Imperial College Press, 2000).

[30] W.-M. Wang, Z.-M. Sheng, Y.-T. Li, L.-M. Chen, S. Kawata, J. Zhang, Monoenergetic electron bunches generated from thin solid foils irradiated by ultrashort, ultraintense circularly polarized lasers, Phys. Rev. ST Accel. Beams **13**, 071301 (2010).

[31] T.-J. Wang, Y. Chen, C. Marceau, F. Theberge, M. Chateauneuf, J. Dubois, and S. L. Chin, High energy terahertz emission from two-color laser-induced filamentation in air with pump pulse duration control, Appl. Phys. Lett. **95**, 131108 (2009).

Figure Captions

Fig.1. Experimental setup. PM1-3, parabolic mirrors; EO, electro-optical detection. The inset illustrates the geometry of the laser interaction with the water column, where THz pulses can be detected at an angle θ rotating from the laser axis (z) in the incident plane xoz.

Fig.2. THz pulses generated from (a) water column with the normal laser incidence and $x_L = 60$ μm, (b) water film with the incident angle of 60°, and (c) air with the normal incidence. The THz pulses are detected by electro-optic sampling and collected at $\theta = 0°$. Plot (d) shows the corresponding spectra.

Fig.3. (a) THz pulses observed in the experimenters with $x_L = \pm 60\mu m$. (b) THz strength as a function of x_L, where experimental and PIC results are shown by dots and line, respectively. (c) PIC results of quasi-static currents $\langle J_x \rangle$ with different x_L, where the broken line in each plots marks the column interface.

Fig.4. THz amplitude as a function of the laser energy, where experimental and PIC results are shown by dots and line, respectively.

Fig.5. Polarization trajectories of the x and y components of THz fields obtained experimentally, where laser polarization angles of $0° - 90°$ are taken, respectively.

Fig.6. THz energy as a function of θ observed in our experiments with $x_L = \pm 60\mu m$, where the detector is located at $x < 0$.

Fig.7. The photo of the water column with a flow rate at 0.015 L/min.

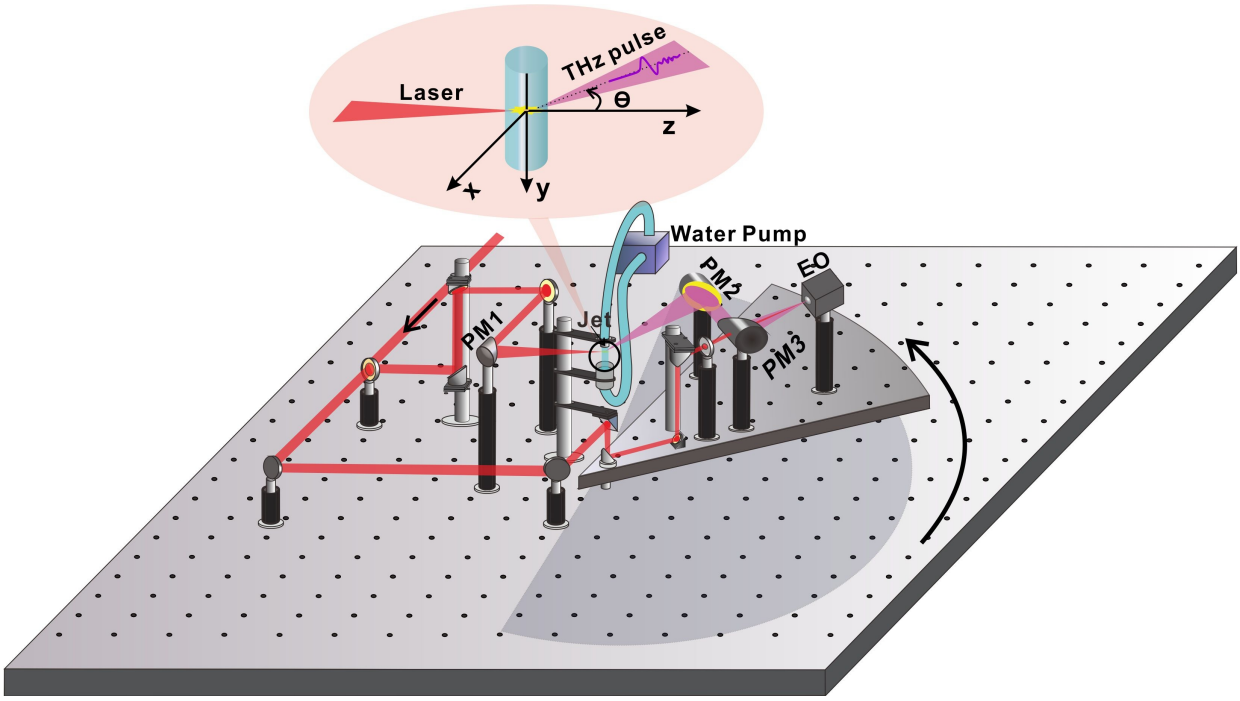

Figure 1 30May2019

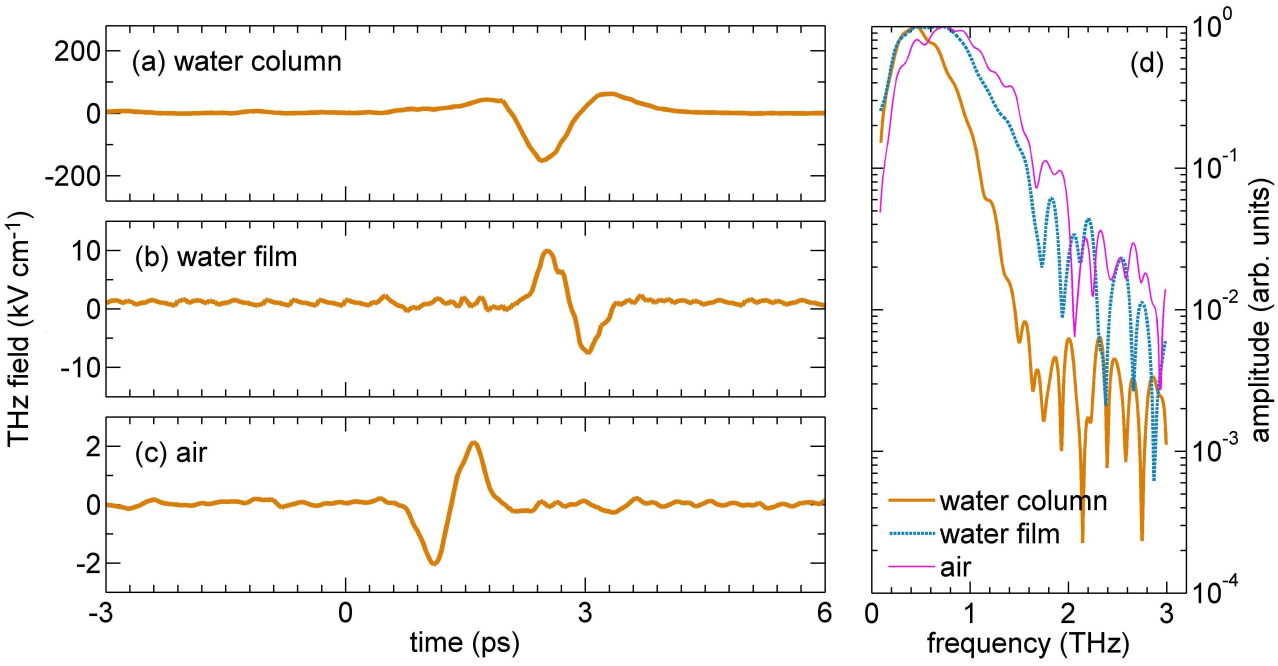

Figure 2 30May2019

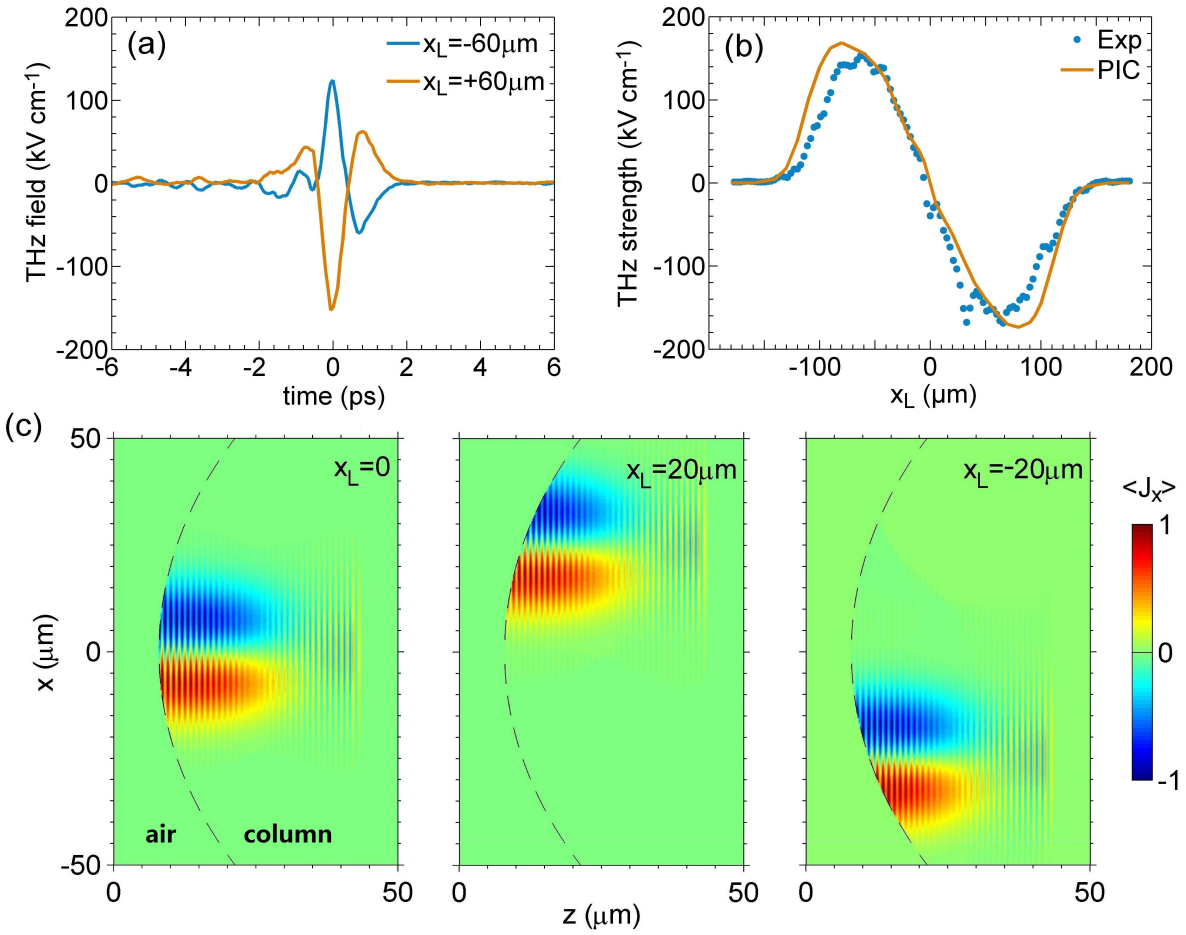

Figure 3 30May2019

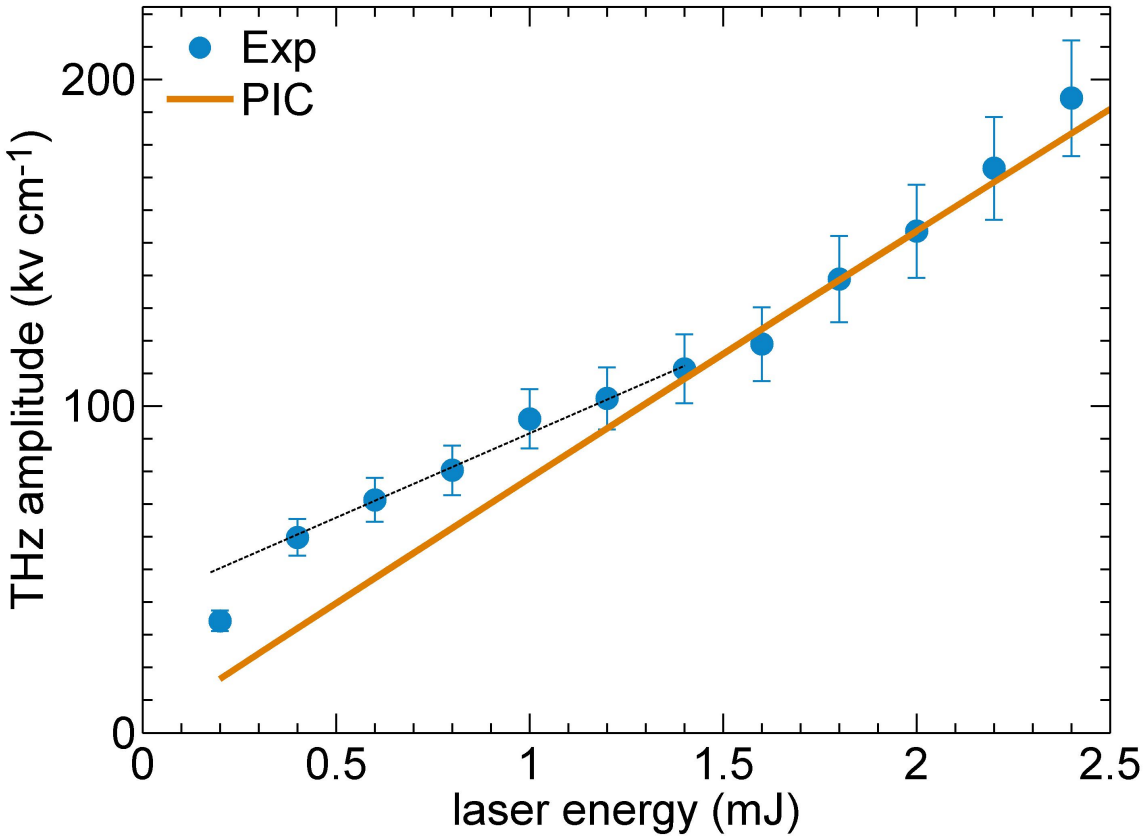

Figure 4 30May2019

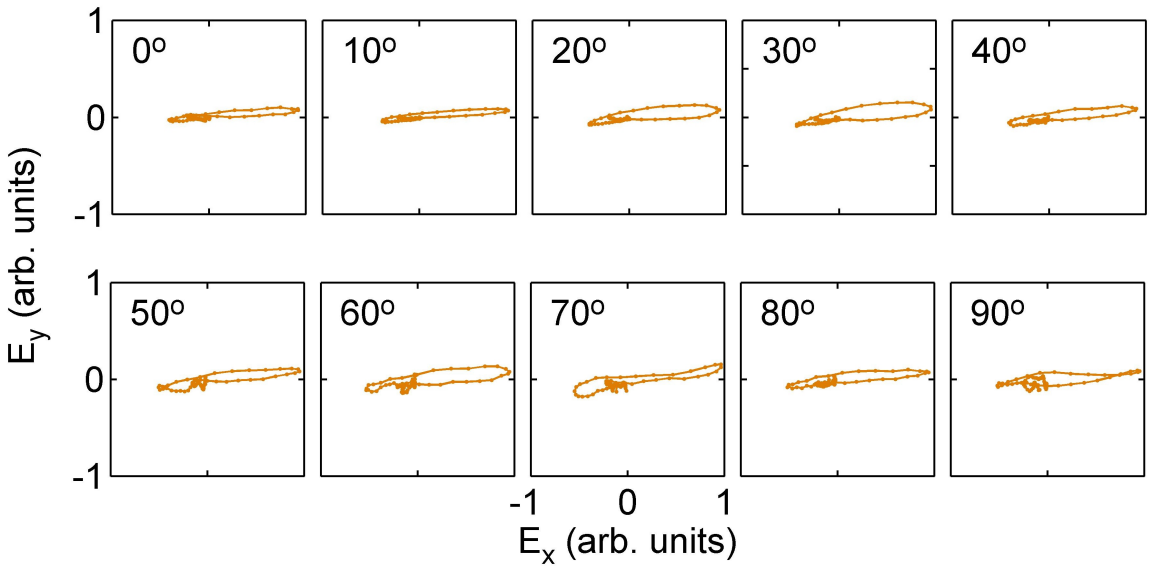

Figure 5 30May2019

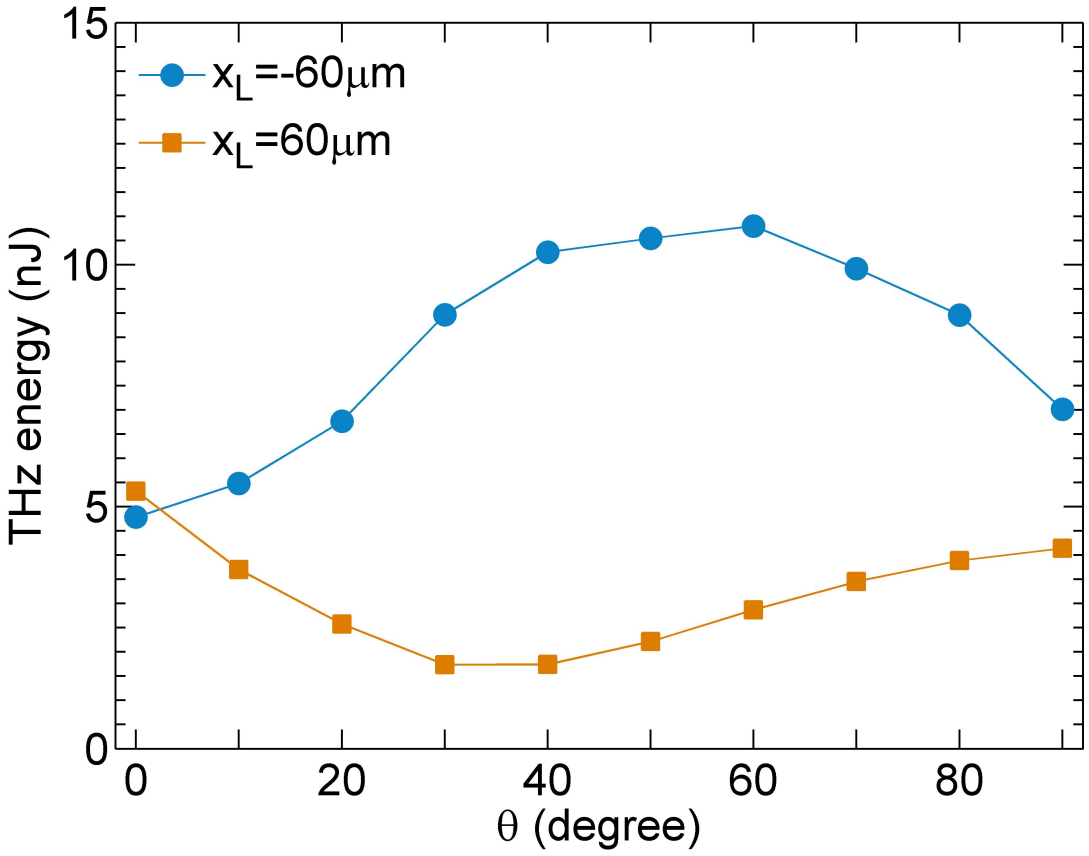

Figure 6 30May2019

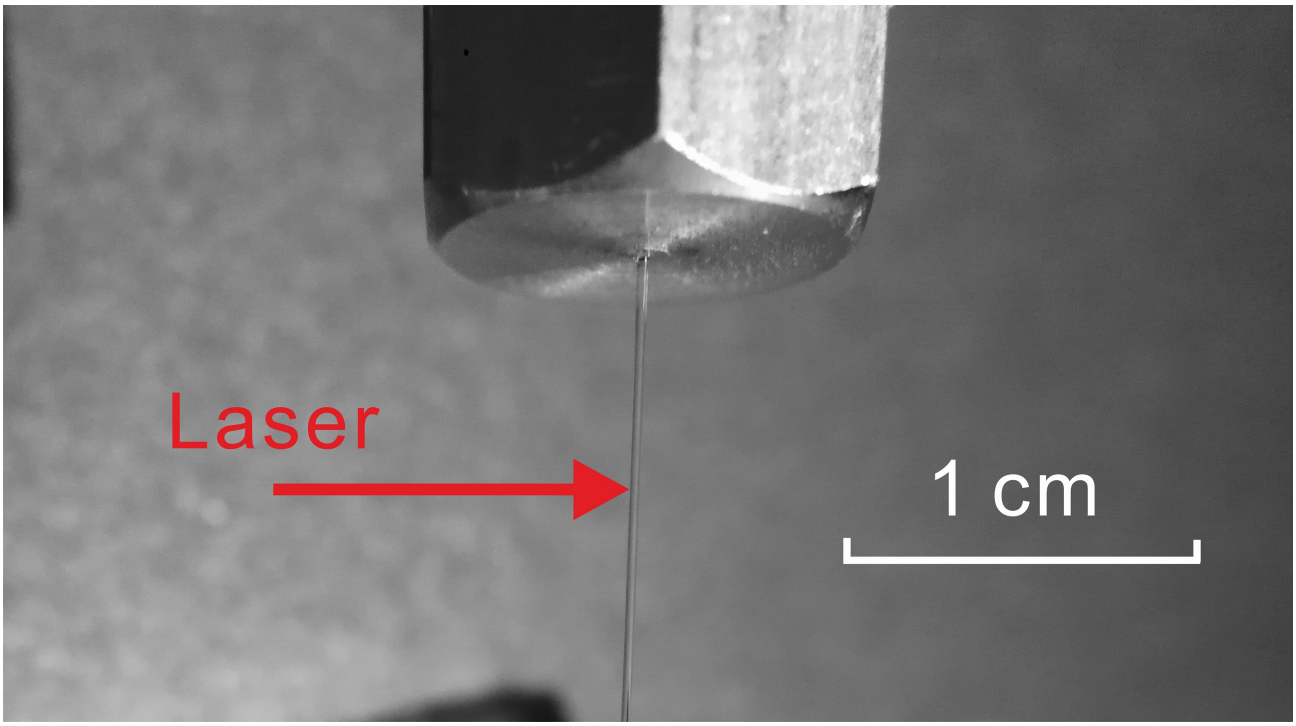

Figure 7 30May2019